ACS APPLIED MATERIALS & INTERFACES

Research Article

www.acsami.org

Fabrication of Unipolar Graphene Field-Effect Transistors by Modifying Source and Drain Electrode Interfaces with Zinc Porphyrin

Mrunal A. Khaderbad,[†] Verawati Tjoa,[‡,§] Manohar Rao,[‡] Rohit Phandripande,[†] Sheri Madhu,[▽] Jun Wei,[§] Mangalampalli Ravikanth,[▽] Nripan Mathews,*[,‡] Subodh G. Mhaisalkar,[‡] and V. Ramgopal Rao*[,†]

[†]Centre of Excellence in Nanoelectronics, IIT Bombay, Mumbai 400076, Maharashtra, India

[‡]School of Materials Science and Engineering, Nanyang Technological University, Singapore 639798

[§]Singapore Institute of Manufacturing Technology, 71 Nanyang Drive, Singapore 638075

[▽]Department of Chemistry, IIT Bombay, Mumbai 400076, Maharashtra, India

ABSTRACT: We report a unipolar operation in reduced graphene oxide (RGO) field-effect transistors (FETs) via modification of the source/drain (S/D) electrode interfaces with self-assembled monolayers (SAMs) of 5-(4-hydroxyphenyl)-10,15,20-tri-(*p*-tolyl) zinc(II) porphyrin (Zn(II)TTPOH) molecules. The dipolar Zn(II)TTPOH molecules at the RGO/platinum (Pt) S/D interface results in an increase of the electron injection barrier and a reduction of the hole-injection barrier. Using dipole measurements from Kelvin probe force microscopy and highest occupied molecular orbital−lowest unoccupied molecular orbital (HOMO−LUMO) calculations from cyclic voltammetry, the electron and hole injection barriers were calculated to be 2.2 and 0.11 eV, respectively, indicating a higher barrier for electrons, compared to that of holes. A reduced gate modulation in the electron accumulation regime in RGO devices with SAM shows that unipolar RGO FETs can be attained using a low-cost, solution-processable fabrication technique.

KEYWORDS: *graphene, transistor, unipolar, self-assembled monolayer, injection barrier*

INTRODUCTION

Graphene, which is a two-dimensional network of carbon atoms, has sparked interest in the research community, because of its unique electrical and mechanical properties. Graphene has a large specific surface area, high intrinsic mobility, a high Young's modulus, and high thermal conductivity.[1,2] Reduced graphene oxide (RGO), which is a solution-processed form of graphene, is being considered in electrical, energy, and sensor applications.[3−5] Its solution processability makes it compatible with spin coating and drop-casting. This allows efficient, low-cost, and large-scale device fabrication virtually on any surfaces.[6−8] The lower carrier mobilities in RGO devices (in comparison to exfoliated graphene),[9] is attributed to the presence of defects and a disconnected network of π-delocalized regions in the carbon atom arrangement. The ambipolar conductance in RGO (and graphene) makes it unsuitable for fabricating logic gates or circuits, since the power consumption is higher in such circuits, compared to unipolar logic. Previous attempts to achieve unipolar transport in graphene include nitrogen doping or the utilization of cobalt electrodes in graphene field-effect transistors (FETs), resulting in asymmetric electron hole currents in the devices.[10,11]

Integrating organic and inorganic materials through a molecular self-assembly provides a route to fine-tune the desired electronic properties of devices at lower costs.[12,13] When self-assembled monolayers (SAMs) with appropriate functional groups are grafted onto metal surfaces, the molecular ordering creates an effective dipole at the metal/SAM interface, which, in turn, tunes the metal work function. Dipolar monolayers of metalloporphyrins are excellent materials for this application, because of their diverse structural motifs and associated electrical, magnetic, optical, and chemical properties. It has been previously demonstrated that metalloporphyrins with different central metal ions can be used to tune the metal-gate work function (and, therefore, the threshold voltage), as well as withstand back-end silicon processing conditions.[14] Charge injection in organic field-effect transistors (OFETs) can also be modulated through the insertion of SAMs, such as in the case of 2,3,5,6-tetrafluoro-7,7,8,8-tetracyanoquinodimethane and alkanethiols.[13,15] In OFETs, the hole and electron injection barrier heights are determined by the difference between the metal electrode work function (φ) and the highest occupied molecular orbital (HOMO) or lowest unoccupied molecular orbital (LUMO) of the semiconductor. In addition, through the integration of dipoles at the metal/semiconductor interfaces, the barrier heights can be modulated, significantly affecting the charge injection.[16,17] However, such a strategy has not been applied in conjunction with graphene-based transistors to modulate charge injection.

Here, we report for the first time, the integration of 5-(4-hydroxyphenyl)-10,15,20-tri-(*p*-tolyl) zinc(II) porphyrin (Zn-(II)TTPOH) SAMs at the electrode interfaces of RGO transistors and have studied their influence on the electrical properties of the transistors. Asymmetric electron−hole currents have been observed in these RGO transistors, which have been correlated to a higher injection barrier for electrons. The injection barriers of electrons and holes have been calculated through HOMO−LUMO energy level measure-

Received: December 1, 2011
Accepted: February 14, 2012
Published: February 14, 2012

dx.doi.org/10.1021/am201691s | ACS Appl. Mater. Interfaces 2012, 4, 1434−1439

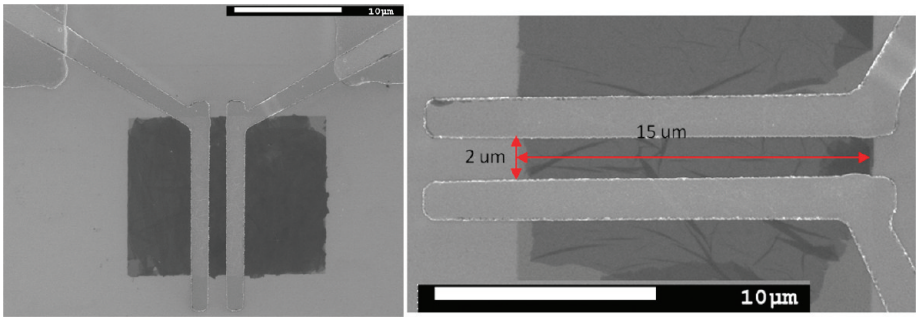

Figure 1. Scanning electron microscopy (SEM) images of fabricated devices.

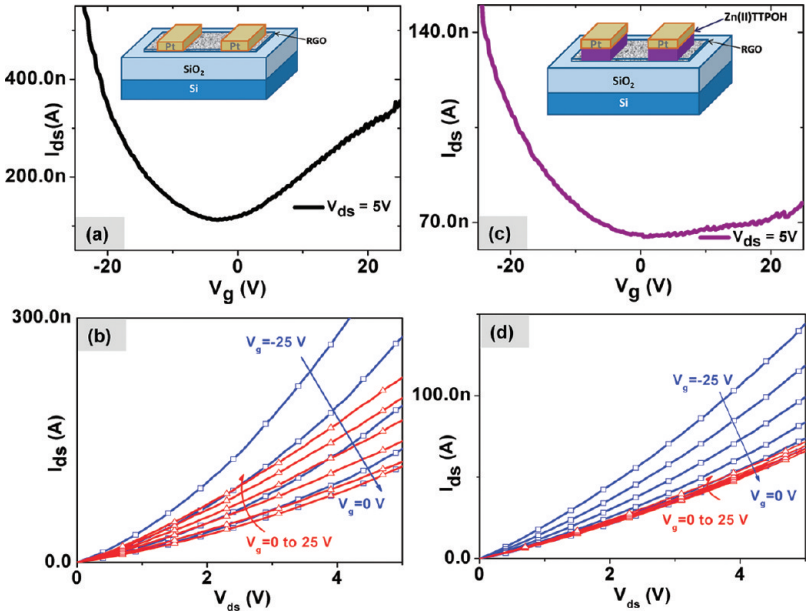

Figure 2. (a) Transfer characteristics of the reduced graphene oxide (RGO) field-effect transistor (FET) for drain-to-source voltage (V_{ds}) = 5 V. (A schematic of the device is shown in the inset, with a channel of 2 μm × 15 μm.) (b) Output characteristics of RGO FETs at different gate voltages. (c) Transfer characteristics of the reduced graphene oxide−self-assembled monolayer (RGO-SAM) FET for V_{ds} = 5 V. (d) Output characteristics of RGO-SAM FETs for different gate voltages (negative gate voltages showing low current modulation).

ments and density functional theory (DFT) calculations of Zn(II)TTPOH, as well as measurements of the dipole associated with the monolayer through Kelvin probe force microscopy (KPFM) techniques.

EXPERIMENTAL SECTION

Synthesis of Graphene and Zn-porphyrin. The synthesis of graphene oxide was performed using the modified Hummer's method, as described elsewhere.[18] The monohydroxy-functionalized porphyrin (TTPOH) was synthesized via the condensation of *p*-hydroxy benzaldehyde, *p*-tolualdehyde, and pyrrole in 1:3:4 ratio refluxing at 100−110 °C in propionic acid for 3 h. The propionic acid was removed by vacuum distillation and the thin-layer chromatography analysis of crude product showed six spots, corresponding to tetratolyl, monohydroxy, (*cis*/*trans*)dihydroxy, trihydroxy, and tetrahydroxy porphyrins. The mixture was subjected to silica gel column chromatography to afford pure 5-(4-hydroxyphenyl)-10,15,20-tri-(*p*-tolyl) porphyrin as a second band, which, upon treatment with $Zn(OAc)_2{\cdot}4H_2O$ in $CHCl_3/CH_3OH$, followed by column chromatographic purification on silica gel, results in pure Zn(II)TTPOH.[19]

SAM Formation. The monolayer of Zn(II)TTPOH was prepared on RGO, following a chemisorption technique that has been reported elsewhere.[14,20] Substrates with RGO were dipped in the solution containing Zn(II)TTPOH molecules dissolved in isopropyl alcohol for 15 min.

Cyclic Voltammetry. The redox chemistry of Zn(II)TTPOH was studied using cyclic voltammetry (CV) at a scan rate of 50 mV/s and differential pulse voltammetry (DPV) at a scan rate of 20 mV/s, using tetrabutylammonium perchlorate (TBAP) as a supporting electrolyte (0.1 M) in dichloromethane. These studies were carried out using a BAS electrochemical system, utilizing the three-electrode configuration, which consists of a glassy carbon (working electrode), platinum wire (auxiliary electrode) and saturated calomel (reference electrode) electrodes. Under these conditions, ferrocene shows a reversible one-electron oxidation wave ($E_{1/2}$ = 0.42 V). The solution was deaerated by bubbling argon gas, and, during the acquisition, argon was slowly flowed above the solution.

Device Fabrication. For electronic measurement, the GO sheet was deposited on a Si/SiO_2 (50 nm) wafer, which was previously plasma-cleaned and modified using aminopropyl triethoxysilane (APTES, Sigma−Aldrich, 99%). GO was deposited through dip coating, and electron-beam (e-beam) lithography (30 keV; the dose is 410 $\mu C/cm^2$) was used to pattern the photoresist coated on the above substrate, forming trenches after development. Subsequently, the substrate was immersed in a bottle containing Zn(II)TTPOH in IPA (0.05 mg/mL) to deposit the porphyrin within the trenches. Samples were then dehydrated at 100 °C for 5 min. Subsequently, platinum metal was sputtered and lift-off was done. This results in porphyrin being sandwiched between the Pt electrode and the graphene. The channel width of the transistor was 15 μm, and the channel length was 2 μm. After removal of the photoresist, GO reduction was then carried

out using hydrazine treatment for 18 h.[21] Eighteen devices with SAM modification were prepared during the study. Data from representative devices are presented here. Figure 1 shows scanning electron microscopy (SEM) images of fabricated devices.

Characterization. The surface morphology and SAM formation were studied using atomic force microscopy (AFM) and Kelvin probe force microscopy (KPFM) on RGO. The KPFM measurement was performed on an Asylum Research Model MF3PD AFM system, using a platinum-coated silicon cantilever (Olympus Model AC240 TM, resonant frequency of ~70 kHz, spring constant of 2 N/m, tip height = 14 μm, and tip radius ≈ 30 nm). Topographic noncontact imaging was performed in frequency modulation mode, while KPFM data was recorded simultaneously in amplitude modulation mode. All scans have been performed in the forward and backward direction, displaying identical topographic, phase, and potential features. KPFM images of the sample were acquired with the tip biased at 3 V at a scan rate of 0.2 Hz, on a typical scan area of 1 μm × 1 μm. The platinum-coated AFM tip was calibrated using sputtered platinum (50 nm thick) on a silicon substrate for work function calculation. A difference of 100 μV was observed between the tip and the sputtered platinum substrate. Electrical measurements were done using a Keithley Model 4200 device on a probe station (Desert Cryogenic, Model TTP-6) under vacuum and ambient conditions.

RESULTS AND DISCUSSION

Figures 2a and 2b display the electrical characteristics of the control RGO devices fabricated without porphyrin pretreatment. As has been observed previously, these RGO-based FETs showed ambipolar transport when measured under vacuum and hole-only transport under ambient conditions.[22] The RGO devices displayed on/off ratios of <10, which is indicative of extensive reduction through the hydrazine treatment and restoration of the π-electron system.

Figure 2b shows the output characteristics of the graphene device, showing the modulation of the electron and the hole transport by the applied gate voltage. Typical hole and electron mobilities calculated from the transfer curves were 2.21×10^{-2} cm^2 V^{-1} s^{-1} and 7×10^{-3} cm^2 V^{-1} s^{-1}, respectively. Similar electrical characterization was also performed in porphyrin-modified transistors (Figure 2c, inset). It is clearly seen from the transfer characteristics that the electron transport in these devices is inhibited. Although there is a small reduction in the hole mobility of these devices, it is not very significant (hole mobility = 1×10^{-2} cm^2 V^{-1} s^{-1}). The clustering of the output characteristics of the porphyrin−graphene device at positive voltages suggests limited gate control.

Since the porphyrin modification is done only at the source and drain electrodes, we examined the energy levels at the graphene/metal interfaces. The inset in Figure 3a shows the energy level diagram of RGO with the Pt electrodes. The work function of RGO[23,24] is between 4.6 eV and 4.9 eV, where, for Pt[25,26] (contact metal), it is ~5.2 eV. The interaction between metal electrodes and graphene has been previously explored in both exfoliated graphene[27] and RGO. In contrast to contact-induced doping in graphene, noninvasive contacts are normally formed on solution-processed graphene in the absence of thermal treatments.[28] Since we have avoided any thermal annealing after the deposition of the Pt electrodes, we assume noninvasive contacts for our discussion. The barrier heights required for charge injection from a metal to the semiconductor with Zn(II)TTPOH interfacial modification can be expressed as[29]

$$\varphi_e = \varphi_M + \Delta\varphi_{dipole} - \chi \quad (1)$$

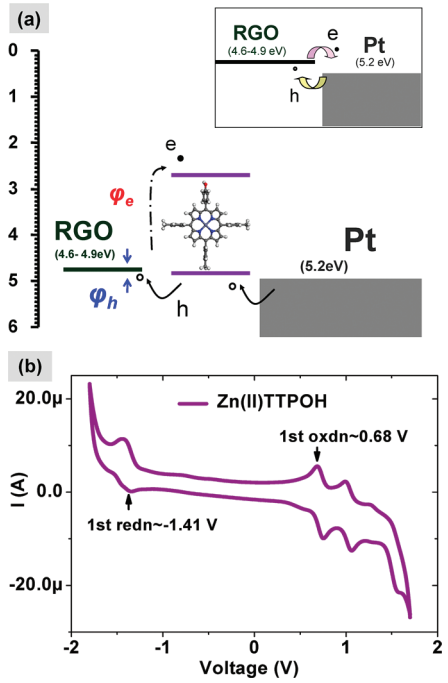

Figure 3. (a) Schematic representation of the SAM-modified source (drain) interface (inset shows the RGO/Pt interface). (b) Cyclic voltammogram of Zn(II)TTPOH.

$$\varphi_h = E_g - (\varphi_M + \Delta\varphi_{dipole} - \chi) \quad (2)$$

where φ_M is the work function of the electrode, χ the electron affinity (LUMO), E_g the band gap of the Zn-porphyrin, and $\Delta\varphi_{dipole}$ the barrier change due to the interface dipole.

To estimate the energy levels of our system, cyclic voltammetry and density functional theory (DFT) calculations of the Zn(II)TTPOH were performed. Different peaks in cyclic voltammograms correspond to different oxidation/reduction states of the material. The onset of oxidation is related to the HOMO energy, corresponding to the removal of electrons. Similarly, the LUMO level can be estimated from the reduction potential. The redox behavior of the Zn(II)TTPOH was investigated by cyclic voltammetry (CV) and differential pulse voltammetry (DPV), using tetrabutylammonium perchlorate (TBAP) as a supporting electrolyte (0.1 M) in dichloromethane (DCM). As seen in Figure 3b, the first oxidation for Zn(II)TTPOH occurs at 0.68 V and first reduction occurs at −1.41 V. These values correspond to a HOMO level of −5.1 eV and a LUMO level of −2.97 eV (based on the fact that ferrocene/ferrocenium is 4.8 eV below the vacuum level with E_{onset} = 0.42 V).[30,31] These values were compared to that from DFT calculations of HOMO and LUMO energy values of the Zn(II)TTPOH molecule.[32] The geometry optimization and subsequent DFT calculations were performed using generalized gradient approximation (GGA) using the nonlocal spin density functional given by Perdew and Wang (PW91). The calculations were spin-unrestricted with DND (double numerical basis set plus d orbitals) as the basis set, which yielded HOMO and LUMO levels of −4.95 eV and −2.44 eV, respectively. These values are comparable to the HOMO and LUMO levels for Zn porphyrin reported elsewhere.[33,34]

To calculate the barrier change due to the dipole ($\Delta\varphi_{dipole}$), surface potential measurements of Zn(II)TTPOH SAM on RGO were performed using KPFM. We use silicon substrates as an in situ reference to measure the potential of the graphene

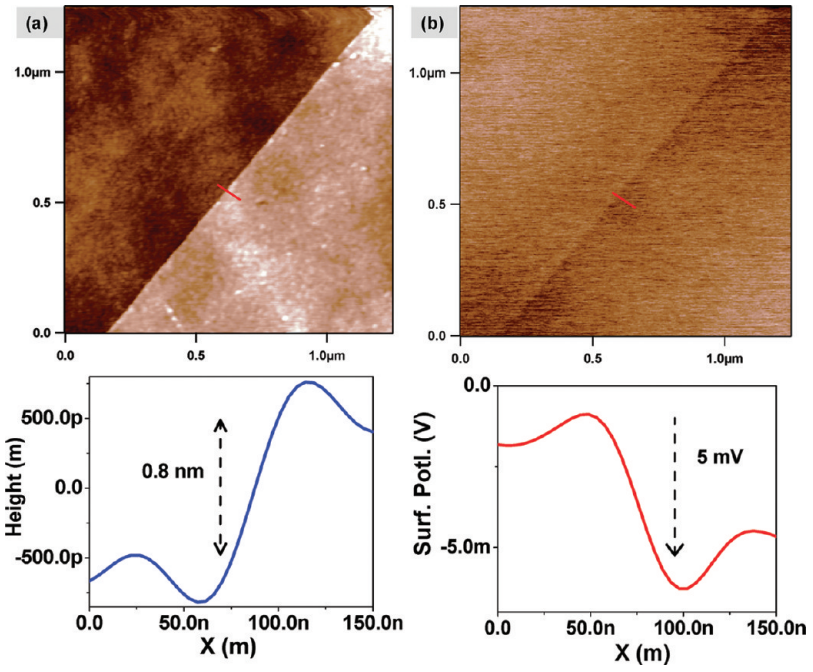

Figure 4. (a) Surface morphology of RGO on silicon. (b) KPFM imaging of RGO on Si showing lower surface potential of RGO, compared to silicon.

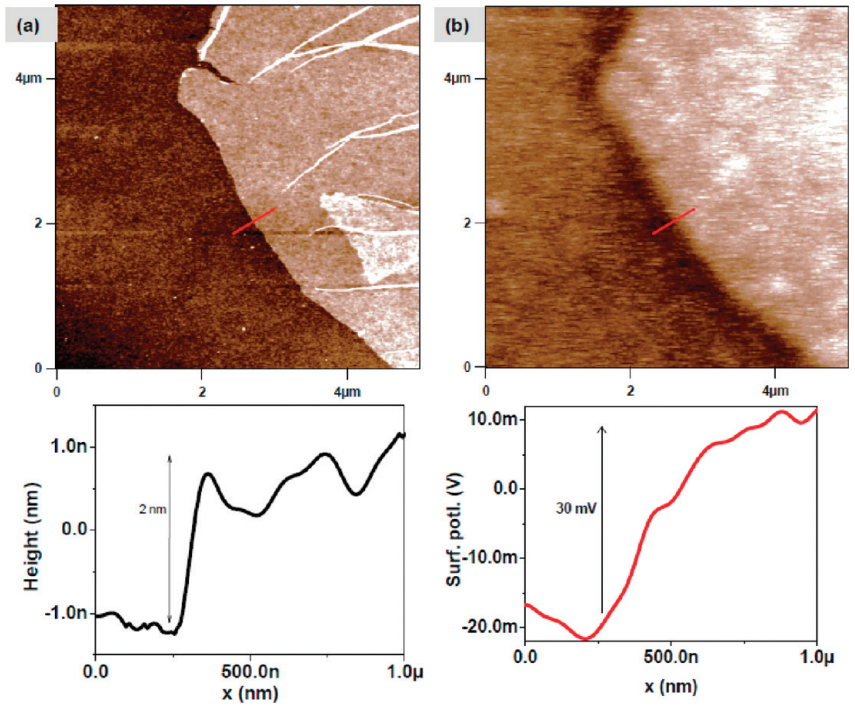

Figure 5. (a) Surface morphology of RGO+SAM on silicon. (b) KPFM imaging of SAM-modified RGO.

and the porphyrin-modified graphene. Measurements of surface potential and surface topography were carried out using KPFM in an ambient environment on single-layer RGO flakes drop-casted onto a silicon substrate. As observed in Figure 4a, the RGO thickness was on the order of 0.8 nm, corresponding to previous reports.[1,6] KPFM analysis on these samples showed a 9 mV *lower* potential of RGO, relative to that of the silicon surface.

Identical measurements were carried out on Zn(II)TTPOH SAM on RGO, which showed a height variation of ∼2 nm, as seen in Figure 5a. In contrast to pristine RGO, the SAM-modified RGO showed a *higher* surface potential (∼30 mV), relative to the silicon surface (see Figure 5b).

This change in potential is due to the dipole moment associated with the Zn central metal ion in the TTPOH molecule. DFT calculations (B3LYP functional, 6-31G(d) basis set) of free-base TTPOH and Zn(II)TTPOH give the values of the overall dipole moments for these molecules as 1.3 D and 2.9577 D, respectively. This is due to the replacement of free-base protons by a metal ion, which introduces an electron-

withdrawing center into the molecule.[35] This metal ion polarizes the σ-orbital network of the porphyrin by accepting electrons from the porphyrin ring, thereby increasing the overall dipole in the molecule.[19,36] This dipole modulates the barrier height at the metal/semiconductor interface.[37,38] In the case of the monolayer system in Figure 5, the molecular density (N) of the SAM is roughly 4×10^{13} cm^{-2}. N can be calculated from the following equation:[39]

$$\Delta V = \left(\frac{N}{\varepsilon_0 \varepsilon_r}\right)\mu \cos(\theta) \tag{3}$$

where μ is the molecule dipole moment (μ = 2.95), N the surface density of molecules, θ the tilt angle of the molecular main axis (relative to the surface normal), ε_r the relative dielectric constant of the porphyrin film (ε_r = 4.2),[40] and ε_0 the vacuum permittivity.

From the KPFM values and HOMO−LUMO levels of Zn(II)TTPOH calculated from CV, φ_e and φ_h can be calculated (from eqs 1 and 2) as 2.2 and 0.11 eV, respectively, showing a higher barrier for electrons, compared to holes (φ_{Pt} ≈ 5.2 eV). At the metal/organic interfaces, the injection current (I) is described as follows:[41,42]

$$I = 4A\Psi^2 N_0 e_0 \mu E \exp\left(-\frac{\varphi_B}{k_B T}\right)\exp(f^{1/2}) \tag{4}$$

where A is the injecting area, N_0 the density of unoccupied sites in the semiconductor, μ the bulk mobility of the injected charge carriers in the organic semiconductor, E the electric field, φ_B the height of the injection barrier, k_B the Boltzmann's constant, and T the temperature. The term Ψ is a slowly varying function of the electric field, and the term f accounts for the reduction in the barrier height due to the electric field at the interface ($f = e^3E/4\pi\varepsilon(k_BT)^2$).

From eq 4, it can be clearly observed that the electron injection is much less, compared to hole injection:

$$I \propto \exp\left(\frac{-\varphi_B}{k_B T}\right)$$

This asymmetry in the injection barriers of electrons and holes is the source of the unipolar behavior in Zn-porphyrin-modified graphene FETs.

CONCLUSIONS

We have shown that it is possible to control electron injection in reduced graphene oxide (RGO) field-effect transistors (FETs) by appropriate interface engineering of source−drain electrodes, using metalloporphyrins. The 5-(4-hydroxyphenyl)-10,15,20-tri-(*p*-tolyl) zinc(II) porphyrin (Zn(II)TTPOH) highest occupied molecular orbital−lowest unoccupied molecular orbital (HOMO−LUMO) energy levels were measured through cyclic voltammetry and the dipole associated with the self-assembled monolayer (SAM) was measured through Kelvin probe force microscopy (KPFM). Estimated electron and hole injection barriers are 2.2 and 0.11 eV, respectively, indicating that Zn(II)TTPOH treatment of RGO at the source/drain interface inhibits electron injection by increasing the barrier height for electrons at the RGO/Pt interface. This work clearly demonstrates that relevant interface modifications using SAM provide a powerful approach to improve the performance of RGO FETs and is critical for applications such as logic gates and integrated circuitry.

AUTHOR INFORMATION

Corresponding Author

*Tel.: +91 22 2576 7456 (V.R.R.), (+65)6790 4626/65141096 (N.M.). Fax: +91 22 25723707 (V.R.R.). E-mail addresses: rrao@ee.iitb.ac.in (V.R.R.), Nripan@ntu.edu.sg (N.M.).

Notes

The authors declare no competing financial interest.

ACKNOWLEDGMENTS

The project was partially supported by A*STAR, Project No.: 102 170 0138.

REFERENCES

(1) Zhu, Y.; Murali, S.; Cai, W.; Li, X.; Suk, J. W.; Potts, J. R. *Adv. Mater.* **2010**, *22*, 3906−3924.
(2) Meyer, J. C.; Geim, A. K.; Katsnelson, M. I.; Novoselov, K. S.; Booth, T. J.; Roth, S. *Nature* **2007**, *446*, 60−63.
(3) Si, Y.; Samulski, E. T. *Nano Lett.* **2008**, *8*, 1679−1682.
(4) Dreyer, D. R.; Park, S.; Bielawski, C. W.; Ruoff, R. S. *Chem. Soc. Rev.* **2010**, *39*, 228−240.
(5) Pumera, M. *Energy Environ. Sci.* **2011**, *4*, 668−674.
(6) Soldano, C.; Mahmood, A.; Dujardin, E. *Carbon* **2010**, *48*, 2127−2150.
(7) Wang, S.; Ang, P. K.; Wang, Z.; Tang, A. L. L.; Thong, J. T. L.; Loh, K. P. *Nano Lett.* **2010**, *10*, 92−98.
(8) Wobkenberg, P. H.; Eda, G.; Leem, D. S.; De Mello, J. C.; Bradley, D. D. C.; Chhowalla, M.; Anthopoulos, T. D. *Adv. Mater.* **2011**, *23*, 1558−1562.
(9) Mkhoyan, K. A.; Contryman, A. W.; Silcox, J.; Stewart, D. A.; Eda, G.; Mattevi, C.; Miller, S.; Chhowalla, M. *Nano Lett.* **2009**, *9*, 1058−1063.
(10) Wang, X.; Li, X.; Zhang, L.; Yoon, Y.; Weber, P. K.; Wang, H.; Guo, J.; Dai, H. *Science* **2009**, *324*, 768−771.
(11) Nouchi, R.; Shiraishi, M.; Suzuki, Y. *Appl. Phys. Lett.* **2008**, *93*, 152104.
(12) Selzer, Y.; Cahen, D. *Adv. Mater.* **2001**, *13*, 508−511.
(13) Abe, Y.; Hasegawa, T.; Takahashi, Y.; Yamada, T.; Tokura, Y. *Appl. Phys. Lett.* **2005**, *87*, 153506.
(14) Khaderbad, M. A.; Roy, U.; Yedukondalu, M.; Rajesh, M.; Ravikanth, M.; Rao, V. R. *IEEE Trans. Nanotechnol.* **2010**, *9*, 335−337.
(15) Asadi, K.; Gholamrezaie, F.; Smits, E. C. P.; Blom, P. W. M.; Boer, Bd. *J. Mater. Chem.* **2007**, *17*, 1947−1953.
(16) Cheng, X.; Noh, Y.-Y.; Wang, J.; Tello, M.; Frisch, J.; Blum, R.-P.; Vollmer, A; Rabe, J. P.; Koch, N.; Sirringhaus, H. *Adv. Funct. Mater.* **2009**, *19*, 2407−2415.
(17) Stoliar, P.; Kshirsagar, R.; Massi, M.; Annibale, P.; Albonetti, C.; de Leeuw, D. M.; Biscarini, F. *J. Am. Chem. Soc.* **2007**, *129*, 6477−6484.
(18) Becerril, H. A.; Mao, J.; Liu, Z.; Stoltenberg, R. M.; Bao, Z.; Chen, Y. *ACS Nano* **2008**, *2*, 463−470.
(19) Gupta, I.; Ravikanth, M. *Coord. Chem. Rev.* **2006**, *250*, 468−518.
(20) Genzer, J.; Efimenko, K. *Science* **2000**, *290*, 2130−2133.
(21) Tjoa, V; Jun, W; Dravid, V; Mhaisalkar, S; Mathews, N. *J. Mater. Chem.* **2011**, *21*, 15593−15599.
(22) Meihua, J.; Hae-Kyung, J.; Woo, J. Y.; Dong, J. B.; Bo, R. K.; Young, H. L. *J. Phys. D: Appl. Phys.* **2009**, *42*, 135109.
(23) Liu, J.; Yin, Z.; Cao, X.; Zhao, F.; Lin, A.; Xie, L.; Fan, Q.; Boey, F.; Zhang, H.; Huang, W. *ACS Nano* **2010**, *4*, 3987−3992.
(24) Li, S.-S.; Tu, K.-H.; Lin, C.-C.; Chen, C.-W.; Chhowalla, M. *ACS Nano* **2010**, *4*, 3169−3174.
(25) Yin, Z.; Wu, S.; Zhou, X.; Huang, X.; Zhang, Q.; Boey, F.; Zhang, H. *Small* **2010**, *6*, 307−312.
(26) Kim, Y.-M.; Lee, J.-S. *Appl. Phys. Lett.* **2008**, *92*, 102901.
(27) Giovannetti, G.; Khomyakov, P. A.; Brocks, G.; Karpan, V. M.; Brink, J.; Kelly, P. J. *Phys. Rev. Lett.* **2008**, *101*, 026803.
(28) Sundaram, R. S.; Gomez-Navarro, C.; Lee, E. J. H.; Burghard, M.; Kern, K. *Appl. Phys. Lett.* **2009**, *95*, 223507.

(29) Ishii, H.; Sugiyama, K.; Ito, E.; Seki, K. *Adv. Mater.* **1999**, *11*, 605−625.
(30) Yen, H.-J.; Lin, K.-Y.; Liou, G.-S. *J. Mater. Chem.* **2011**, *21*, 6230−6237.
(31) Al-Ibrahim, M.; Roth, H. K.; Zhokhavets, U.; Gobsch, G.; Sensfuss, S. *Sol. Energy Mater. Sol. Cells* **2005**, *85*, 13−20.
(32) Delley, B. *J. Chem. Phys.* **2000**, *113*, 7756−7764.
(33) Koo, J.-R.; Lee, H.-S.; Ha, Y.; Choi, Y.-H.; Kim, Y. K. *Thin Solid Films* **2003**, *438*, 123−127.
(34) Liao, M.-S.; Scheiner, S. *J. Chem. Phys.* **2002**, *117*, 205−219.
(35) Karweik, D. H.; Winograd, N. *Inorg. Chem.* **1976**, *15*, 2336−2342.
(36) Oakes, R. E.; Bell, S. E. J. *J. Phys. Chem. A* **2003**, *107*, 10953−10959.
(37) Cai, Q. J.; Chan-Park, M. B.; Zhou, Q.; Lu, Z. S.; Li, C. M.; Ong, B. S. *Org. Electron.* **2008**, *9*, 936−943.
(38) Cui, X.; Freitag, M.; Martel, R.; Brus, L.; Avouris, P. *Nano Lett.* **2003**, *3*, 783−787.
(39) Campiglio, P.; Campione, M.; Sassella, A. *J. Phys. Chem. C* **2009**, *113*, 8329−8335.
(40) Savenije, T. J.; Moons, E.; Boschloo, G. K.; Goossens, A.; Schaafsma, T. J. *Phys. Rev. B* **1997**, *55*, 9685−9692.
(41) Schidleja, M.; Melzer, C.; Seggern, H. V. *Adv. Mater.* **2009**, *21*, 1172−1176.
(42) Scott, J. C.; Malliaras, G. G. *Chem. Phys. Lett.* **1999**, *299*, 115−119.